A Design to Investigate the Influence of Light on the Sensitivity of Capacitive Gas Sensors

D.J.J. Borggreven
A.M.A. Feenstra
A.J. De Jong
J.C. Wooning

Supervisors: M. Kabatas, T. Shen, M. K. Ghatkesar, P.G. Steeneken

Mechanical Engineering BSc

A Thesis Submitted to ME Faculty Delft University of Technology, to obtain the degree of Bachelor of Science
June, 2025

TU Delft

***Abstract*—Early detection of plant diseases is crucial to minimize crop losses and reduce the usage of pesticides. Electronic Nose (E-Nose) detect volatile organic compounds (VOCs) emitted by stressed or diseased plants, and one such device is a pixelated capacitive sensor (PCS). We designed and built a setup to investigate the influence of light (wavelength and intensity) on the sensitivity of a functionalized PCS for VOCs detection. Our test results indicate that UV illumination, particularly at 375 nm, enhances the sensitivity of the PCS, with a 3-fold enhancement compared to dark conditions. The sensor showed fast saturation (<1 min) and recovery (<2 min) times , confirming the effectiveness of the chamber design for repeatable gas exposure.**

***Keywords*–E-nose, VOC gas sensor, gas testing chamber, photodetector,**

I. Introduction

Each year, up to 40% of global crop yields are lost due to pests, therefore early detection of plant stress and disease is essential to reduce such losses [1]. A promising method for early stress detection in plants is the monitoring of volatile organic compounds (VOCs). The VOCs released by plants depend on various physico-chemical factors. When a plant is infected with a disease, the VOC profile differs from that of a healthy plant. Detecting these changes in VOCs enables real-time disease identification and can help prevent the spread of plant diseases

One technology capable of detecting VOCs is the electronic nose (E-nose) sensor. A range of different mechanisms for such an E-nose have been developed, including conductivity sensors, piezoelectric sensors, optical sensors, and capacitive sensors. In this work, we focus on a capacitive-based approach using a Pixelated Capacitive Sensor (PCS) [2].

The PCS consists of multiple electrodes and a layer of sensing ink. The response of capacitive sensors depend on both solubility interactions (i.e., how much of the VOC partitions into the sensing ink) and the dielectric constants of both the sensing ink and the VOC [3]. However, currently one of the challenges is the limited sensitivity of gas sensors, which can impact early detection and reliability. Interestingly, gas sensors exposed to light illumination have shown promising improvements, including higher response levels and faster adsorption and desorption times [4–9]. Since the optimal optical wavelength depends on the bandgap of the sensing material, understanding the influence of light across different wavelengths is crucial and has not yet been investigated for the PCS chip. To enable this, a test chamber is required to study these effects under controlled conditions[10].

This need forms the basis of the current project, which is guided by the following research question: How to design and build a VOC compatible test chamber with optimized gas flow rate range and light-tight illumination?

This work describes the design and construction of a custom test chamber to study the influence of light exposure on VOC sensor performance. The chamber accommodates various gas types, light intensities, and wavelengths. Measurements were performed with and without illumination to assess its effect on sensor sensitivity and reliability.

The paper is structured as follows: Section II provides background on VOC sensing and sensor mechanisms. Section III describes the design process. Section IV describes the methodology. Section V presents and discusses the results, followed by a discussion and conclusions in Section VI and VII. This research was conducted as part of the Bachelor End Project by third-year Mechanical Engineering students at TU Delft.

II. Theory

A. VOC Detection

As mentioned before, a PCS can detect plant stress and disease by sensing the specific VOCs that plants release in response to their state. The sensor consists of interdigitated electrodes placed on a substrate with a sensing ink in between. When no VOCs interact with the sensing layer (Fig. 1a), a baseline capacitance exists between the electrodes and the sensing ink.

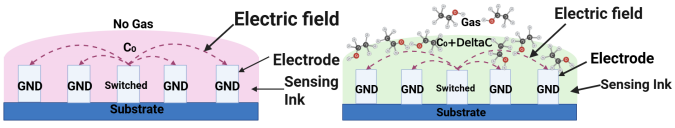

Fig. 1. Working principle of the PCS for sensing the VOCs

When VOCs are present, the relative permittivity ϵ_r of the sensing ink changes due to the adsorption of VOC molecules (Fig. 1b). This alters the capacitance between the electrodes and the sensing ink. This way the presence of a VOC can be identified by a deviation from the baseline signal, while the magnitude and pattern of this change can offer information about the type of VOC, since different compounds interact differently with the sensing material.

B. Effects of light on sensor sensitivity

As noted earlier, the sensitivity of gas sensors, as well as the rates of adsorption and desorption, can be enhanced through light illumination [4–9]. When the energy of the incoming photons exceeds the bandgap energy, of the sensing material, electrons are excited from the valence band to the conduction band, creating free charge carriers. This leads to an increase in electrical conductivity and changes the dielectric properties of the material. As the relative permittivity ϵ_r changes, the capacitance between the sensor electrodes is also affected, changing its sensitivity to VOCs. This behaviour can be described by using the Maxwell equation (1) [11]:

$$\nabla \times \mu_r^{-1}(\nabla \times \mathbf{E}) - k_0^2(\epsilon_r - j\frac{\sigma}{\omega\epsilon_0})\mathbf{E} = \mathbf{0} \quad (1)$$

Where, the term $j\frac{\sigma}{\omega\epsilon_0}$ represents the imaginary part of the complex permittivity, which describes the dielectric loss. Any change in conductivity σ [S/m] due to external light affects this term, and thus the electric field $\mathbf{E}$ [V/m] across the sensor and thus the capacitance of the PCS. μ_r is the relative permeability, describing the material's magnetic response. k_0 [1/m] is the vacuum wave vector ($k_0 = \frac{\omega}{c}$), which serves as the reference scale for electromagnetic wave propagation, it determines the periodicity that gets modified by the material properties. ω [rad/s] and ϵ_0 are the angular frequency and vacuum permittivity, respectively, needed to convert the material's conductivity σ into proper electromagnetic units for the wave equation.

C. Chamber design

Optimizing the gas testing chamber for reliable sensor response involves consideration of volume, sensor placement, and gas flow direction. Lopez Jr. et al. [12] demonstrated that a smaller chamber volume (1 mL cap chamber vs. 400 mL conventional chamber) significantly improves sensor performance, leading to 154% faster response and 86.9% faster recovery due to quicker gas exchange and reduced stagnant regions.

III. Design

For the gas-sensing tests with the VOCs and the E-nose, a test chamber was designed following its pre-determined design criteria. The chamber needed to have a volume of <3 mL, see II-C, UV- and chemical resistance and be airtight to ensure effective and reliable testing. Also, a window needed to be added for testing with illumination. The criteria of the window is a broad wavelength range from deep UV, 200nm, to near IR, 1000nm, wavelengths, and a transparency percentage higher than 85% to minimize the light intensity loss.

A. Geometry of the test chamber

The test chamber has a volume of approximately 0.92 mL, kept small to minimize dead zones and ensure efficient gas flow. It is 3D-printed with PEEK, chosen for its excellent UV and chemical resistance. To minimize the LED-sensor distance, for maximum light intensity, the inlet and outlet are positioned horizontally. The final design of the test chamber is shown in Fig.2

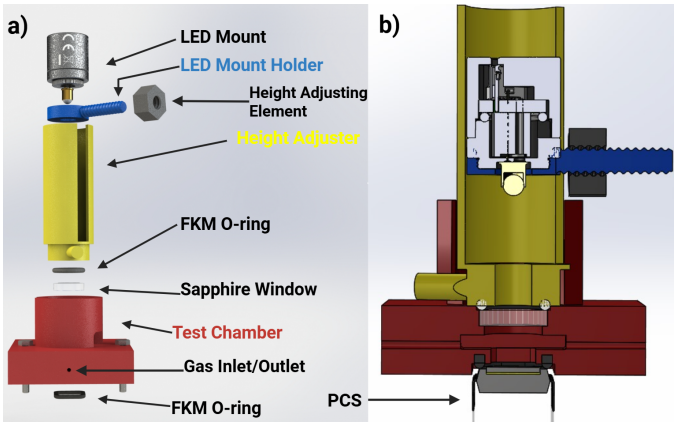

Fig. 2. a) Exploded view test chamber b) Cross-section test chamber

B. Light sources

For the light source, three LEDs with wavelengths of 375 nm, 395 nm, and 645 nm were chosen to evaluate the broad spectral range from UV to visible red light. The LEDs are mounted into a USB powered holder, which then will be screwed into a height adjustable 3D-printed holder positioned directly above the sensor, thereby maximizing its efficiency.

The LED holder's height can be vertically adjusted along a rails. Once positioned, the holder is secured in place using a 3D-printed locking nut.

C. Sealing and window

When interlocked with a bajonet lock onto the chamber, the 3D-printed height adjuster presses a Fluorelastomer-Kautschuk (FKM) O-ring against the sapphire window ,with a >88% transparency from 275–5500 nm, to form an airtight seal. A second FKM O-ring is placed around the chip at the bottom of the chamber to reinforce sealing. FKM O-rings are used due to their excellent resistance to gases, chemicals, and UV light.

To prevent external light from reaching the sensor surface, a black 3D-printed cap is placed over the test chamber at the start of each measurement.

IV. Methodology

Testing begins with leakage and light illumination checks to ensure chamber sealing and window transparency at various heights. Chamber and sensor dynamics are analyzed using COMSOL Multiphysics. Finally, the effect of light intensity and wavelength on sensor response is evaluated.

A. Light intensity tests

The light intensity was measured across different wavelengths and heights, both with and without a window. In addition, the transparency of the Sapphire window was also evaluated to verify the reported 88% value (see III-C).

Table I presents the measured light intensities (in lux) at three wavelengths and various heights, with (top) and without

(bottom) a sapphire window. At all wavelengths, intensity decreases with height. The transparency can be calculated by finding the ratio between the two tables, this corresponds with the given 88% reported in Chapter III-C.

TABLE I
LIGHT INTENSITY TESTS

Light Intensity Results (lux)					
WL (nm)	**20mm**	**40mm**	**60mm**	**80mm**	**I(mW)**
375	31	9	2	0	1
395	2035	701	306	153	6
645	5796	1931	807	363	16
375	36	10	3	0	1
395	2175	739	342	177	6
645	6116	2018	902	416	16

B. Gas sensing setup

Ethanol vapor was generated by bubbling air through a 50mL container of liquid ethanol and delivered to the sensing chamber via tubing at a flow rate of 1mL/min. For each LED wavelength, a sensing cycle was performed consisting of three phases: 10 minutes in the dark with ethanol vapor (baseline), followed by 20 minutes of exposure to the same vapor under illumination. For safety reasons the sensor was printed with UV-curable ink, as the ink does not contain nanoparticles and adheres well to the surface. responses were recorded in real time via a PCB-connected interface and analyzed at maximum light intensities for each wavelength.

V. RESULTS

A. Comsol simulation results

To optimize the design to ensure a smooth airflow through the test chamber, different simulations have been conducted using the Comsol Multiphysics module for laminar flow. Moreover, the effect of illumination on the electrical behavior of different sensor materials has been investigated using a photo detector model with the semiconductor and the EM-wave module.

1) Streamlines: To ensure accurate sensor readings, the flow within the chamber was designed to be laminar. The maximum Reynolds number calculated was 12.2 at the inlet, confirming laminar flow and the absence of recirculations. This is further supported by the concentration streamlines shown in Figure 3, which depict ethanol (500 ppm) flowing uniformly over the sensor surface for 60 seconds at a rate of 5 mL/min, with no signs of turbulence.

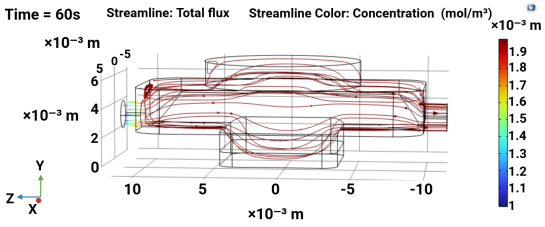

Fig. 3. Concentration streamlines in saturated state

2) Filling and emptying time: For fast and efficient testing, it is important that the chamber reaches the set point concentration and can be emptied quickly. Figure 4 shows the concentration at the sensor surface and outlet during exposure to 500ppm of ethanol for 60 seconds at a flow rate of 5 mL/min. The target concentration reaches the sensor surface in approximately 40 seconds and goes back to zero within 60 seconds after the injection of ethanol ends, demonstrating a rapid response suitable for efficient testing cycles.

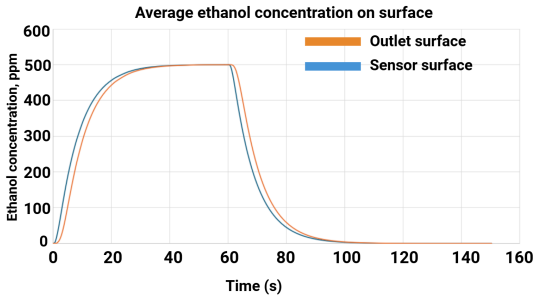

Fig. 4. Ethanol concentration on the outlet and sensor surface during an injection of 500ppm at 5ml/min for 60 s

3) Effect light on electrical response material: Different materials can be printed on the sensor and their bandgap is expected to influence the sensor's electrical response. Different materials with varying bandgaps E_g and corresponding wavelengths λ_g were simulated: CuO (1033 nm), GaAs (870 nm), GaN (380 nm), and ZnO (368 nm). The photodetector model simulates light absorption at $\lambda \leq \lambda_g$, generating electron-hole pairs that increase conductivity. Resistance measurements showed minimal resistance around λ_g due to increased free charge carriers, with higher intensity broadening the response curve as more photons increase absorption probability. Simulations were performed between λ_{min} and λ_{max} (Comsol's maximum range) to avoid division-by-zero errors, using literature-based intensities of 100-500 W/m^2.

B. Gas sensing results

Figure 5 presents a comprehensive overview of ethanol gas sensing behavior of a UV-curable ink-based photodetector under controlled flow and illumination conditions. Panel (a) shows the sensor response to ethanol gas (introduced at 1 mL/min), with air serving as the baseline gas. Upon exposure to ethanol, the signal increases rapidly, and when the gas flow is switched back to air, the signal returns to baseline. This confirms the efficient design of the gas delivery chamber, ensuring rapid analyte exposure and effective purging.

Panels (b) and (c) explore the photoactivation behavior of the sensor under LED light sources of 375 nm (black), 395 nm (red), and 645 nm (blue). The sensor response, represented as ΔADC (a.u.) normalized by sensor signal, is plotted with intentional Y-axis offsets for visual clarity. Panel (b) shows only a linear increasement at the UV-LED, this suggests that shorter wavelengths ($<$ 400, UV) such as 375 nm are effective for activating the UV-curable ink, due to better absorption and

stronger interaction with the sensor material. These findings support the use of 375 nm light as a promising and safe choice for UV activation.

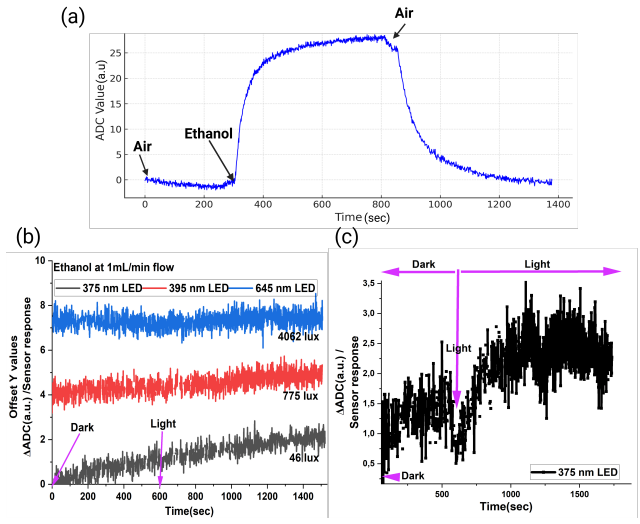

Fig. 5. (a) Ethanol sensing under dark conditions with switching between Air and ethanol flow, confirming rapid gas delivery and full baseline recovery. (b) Comparative sensor responses under different illumination wavelengths (375 nm, 395 nm, 645 nm LEDs) under dark/light cycling conditions. (c) Zoomed-in plot for the 375 nm LED response, highlighting light-induced enhancement.

Panel (c) provides a zoomed view of the 375 nm LED case. The signal remains near baseline in dark conditions but exhibits a 3-fold enhancement response upon illumination, confirming the ink's UV-sensitive nature. This suggests 375 nm is the most photo-efficient activation wavelength due to the printed materials' band gap, enabling light-triggered gas sensing with minimal power input.

Collectively, these results demonstrate that UV-curable ink-based sensors, when paired with suitable UV illumination (e.g., 375 nm), offer promising avenues for highly sensitive, light-activated gas detection.

VI. Discussion

While the inlet maintained an airtight seal, approximately 10% leakage occurred around the sensor surface due to inadequate O-ring contact. Testing different O-ring dimensions in future iterations could eliminate this leakage and achieve complete airtightness. Furthermore, the incorporation of heat regulation in future designs is recommended to ensure more consistent conditions and allow testing of the influence of different temperatures. High ethanol concentrations in the current setup are suspected to have impeded light transmission to the sensor surface. Therefore, lower flow rates or lower concentrations should be used in future tests to improve light penetration and sensor performance. Finally, we were limited to three different wavelengths; however, to determine the optimal wavelength, integrating a light source with a continuous spectrum would be beneficial.

VII. Conclusion

This study presents the successful design, fabrication and testing of a custom gas-sensing chamber to investigate the influence of light on PCS sensitivity for VOC detection. The chamber achieved compact volume (< 1 mL), laminar flow for efficient gas exchange, and featured a sapphire window with transparency in the 375–5500 nm wavelength range for controlled illumination. COMSOL simulations and experiments demonstrated fast gas saturation and purging, enabling repeatable testing conditions. Sensor tests under ethanol exposure showed clear response enhancement when illuminated, particularly under UV light. Despite lower power, the 375 nm LED yielded 3-fold enhancement, indicating the UV-curable sensing ink's bandgap aligns well with this wavelength, confirming light-assisted activation's potential even at low illumination intensities.

The findings highlight that controlled UV illumination enhances capacitive VOC sensor responsiveness and sensitivity, opening new avenues for optimizing light conditions in next-generation E-nose systems for real-time plant health monitoring.

Acknowledgment

We are very thankful to our supervisors Murat Kabatas, Tao Shen, Murali K. Ghatkesar and Peter Steeneken for their guidance and advice, ME Faculty Workshop and the PME department for their support for fabrication, and Gerard Verbiest and Angelo Accardo for their feedback during the colloquium and jury presentation.

References

[1] FAO, "About fao's work on plant production and protection," *Plant production and protection*, 2023. [Online]. Available: https://www.fao.org/plant-production-protection/about/en

[2] F. Widdershoven, "Pixelated capacitive sensors (pcs) for embedded multi-sensing," NXP Semiconductors Delft University of Technology, Tech. Rep.

[3] S. Jenkins, *Hansen Solubility Parameters (HSP)*, 2011, unspecified publisher.

[4] Geng, Q. et al., "Gas sensing property of ZnO under visible light irradiation at room temperature," *Sensors and Actuators B Chemical*, vol. 188, pp. 293–297, 7 2013. [Online]. Available: https://doi.org/10.1016/j.snb.2013.07.001

[5] Paul, S. et al., "Enhancing room-temperature gas sensing performance of metal oxide semiconductor chemiresistors through 400 nm UV photoexcitation," *Sensors and Actuators Reports*, vol. 7, p. 100194, 4 2024. [Online]. Available: https://doi.org/10.1016/j.snr.2024.100194

[6] Comini, E. et al., "UV light activation of tin oxide thin films for NO2 sensing at low temperatures," *Sensors and Actuators B Chemical*, vol. 78, no. 1-3, pp. 73–77, 8 2001. [Online]. Available: https://doi.org/10.1016/s0925-4005(01)00796-1

[7] Zhang, C. et al., "Room temperature responses of visible-light illuminated WO3 sensors to NO2 in sub-ppm range," *Sensors and Actuators B Chemical*, vol. 181, pp. 395–401, 2 2013. [Online]. Available: https://doi.org/10.1016/j.snb.2013.01.082

[8] Wang, X. et al., "Flexible and transparent sensors for ultra-low NO2 detection at room temperature under visible light illumination," *Journal of Materials Chemistry A*, vol. 8, no. 29, pp. 14 482–14 490, 1 2020. [Online]. Available: https://doi.org/10.1039/d0ta02934c

[9] Liu, B. et al., "Room-Temperature NO2 Gas Sensing with Ultra-Sensitivity Activated by Ultraviolet Light Based on SnO2 Monolayer Array Film," *Advanced Materials Interfaces*, vol. 6, no. 12, 5 2019. [Online]. Available: https://doi.org/10.1002/admi.201900376

[10] Sadredini, A. R. et al., "Intensity modulation of uv light in gas sensor array to discriminate several analytes at room temperature," *IET Science, Measurement Technology*, vol. 18, pp. 65–73, 2024. [Online]. Available: https://digital-library.theiet.org/doi/abs/10.1049/smt2.12167

[11] "Frequency domain equation." [Online]. Available: https://doc.comsol.com/5.5/doc/com.comsol.help.rf/rf_ug_radio_frequency.07.78.html#1310050

[12] Lopez, L. et al., "Influence of chamber design on the gas sensing performance of graphene field-effect-transistor," *SN Applied Sciences*, vol. 2, no. 7, 6 2020. [Online]. Available: https://doi.org/10.1007/s42452-020-2676-5